

Large spatial shifts of reflected light beam off biaxial hyperbolic materials

Jia-Guo Shen(沈加国), Syed-ul-hasnain Bakhtiar(哈思内恩), Hao-Yuan Song(宋浩元), Sheng Zhou(周胜), Shu-Fang Fu(付淑芳), Xuan-Zhang Wang(王选章), Xuan Wang(王暄), and Qiang Zhang(张强)
Citation: Chin. Phys. B, 2023, 32 (**11**): 114206. DOI: 10.1088/1674-1056/acd526
Journal homepage: http://cpb.iphy.ac.cn; http://iopscience.iop.org/cpb

What follows is a list of articles you may be interested in

Nonlinear perturbation of a high-order exceptional point: Skin discrete breathers and the hierarchical power-law scaling

Hui Jiang(江慧), Enhong Cheng(成恩宏), Ziyu Zhou(周子榆), and Li-Jun Lang(郎利君)
Chin. Phys. B, 2023, 32 (**8**): 084203. DOI: 10.1088/1674-1056/accb47

High power, widely tunable femtosecond MgO:PPLN optical parametric oscillator

Jinfang Yang(杨金芳), Chong Wang(王翀), Weijun Ling(令维军), Jingwen Xue(薛婧雯), Xiaojuan Du(杜晓娟), Wenting Wang(王文婷), Yuxiang Zhao(赵玉祥), Feiping Lu(路飞平), Xiangbing Li(李向兵), Jiajun Song(宋贾俊), Zhaohua Wang(王兆华), and Zhiyi Wei(魏志义)
Chin. Phys. B, 2023, 32 (**7**): 074204. DOI: 10.1088/1674-1056/accd59

Two-photon absorption of $FAPbBr_3$ perovskite nanocrystals

Xuanyu Zhang(张轩宇), Shuyu Xiao(肖书宇), Xiongbin Wang(王雄彬), Tingchao He(贺廷超), and Rui Chen(陈锐)
Chin. Phys. B, 2023, 32 (**6**): 064212. DOI: 10.1088/1674-1056/acb203

Giant saturation absorption of tungsten trioxide film prepared based on the seedless layer hydrothermal method

Xiaoguang Ma(马晓光), Fangzhen Hu(胡芳珍), Xi Chen(陈希), Yimeng Wang(王艺盟), Xiaojian Hao(郝晓剑), Min Gu(顾敏), and Qiming Zhang(张启明)
Chin. Phys. B, 2023, 32 (**3**): 034212. DOI: 10.1088/1674-1056/acaf2a

Tunable enhanced spatial shifts of reflective beam on the surface of a twisted bilayer of hBN

Yu-Bo Li(李宇博), Hao-Yuan Song(宋浩元), Yu-Qi Zhang(张玉琦), Xiang-Guang Wang(王相光),Shu-Fang Fu(付淑芳), and Xuan-Zhang Wang(王选章)
Chin. Phys. B, 2022, 31 (**6**): 064207. DOI: 10.1088/1674-1056/ac3733

Large spatial shifts of reflected light beam off biaxial hyperbolic materials

Jia-Guo Shen(沈加国)[1], Syed-ul-hasnain Bakhtiar(哈思内恩)[2], Hao-Yuan Song(宋浩元)[1], Sheng Zhou(周胜)[1], Shu-Fang Fu(付淑芳)[1,2,†], Xuan-Zhang Wang(王选章)[1], Xuan Wang(王暄)[3], and Qiang Zhang(张强)[1,‡]

[1] *Key Laboratory for Photonic and Electronic Bandgap Materials, Chinese Ministry of Education, and School of Physics and Electronic Engineering, Harbin Normal University, Harbin* 150025, *China*

[2] *School of Integrated Circuits, Engineering Research Center for Functional Ceramics, Wuhan National Laboratory for Optoelectronics, Huazhong University of Science and Technology, Wuhan* 430030, *China*

[3] *Key Laboratory of Engineering Dielectrics and Its Application, Ministry of Education, Harbin University of Science and Technology, Harbin* 150080, *China*

(Received 13 March 2023; revised manuscript received 11 May 2023; accepted manuscript online 12 May 2023)

Many optical systems that deal with polarization rely on the adaptability of controlling light reflection in the lithography-free nanostructure. In this study, we explore the Goos–Hänchen (GH) shift and Imbert–Fedorov (IF) shift in a biaxial hyperbolic film on a uniaxial hyperbolic substrate. This research statistically calculates and analyzes the GH shift and IF shift for the natural biaxial hyperbolic material (NBHM). We select the surface with the strongest anisotropy within the NBHM and obtain the complex beam-shift spectrum. By incorporating the NBHM film, the GH shift caused by a transversely magnetic incident-beam on the surface increases significantly compared with that on the uniaxial hyperbolic material. The maximum of GH shift can reach $86\lambda_0$ at about 841 cm^{-1} when the thickness of NBHM is 90 nm, and the IF shift can approach $2.7\lambda_0$ for a circularly-polarized beam incident on a 1700-nm-thick NBHM. It is found that the spatial-shift increases when a highly anisotropic hyperbolic polariton is excited in hyperbolic material, where the shift spectrum exhibits an oscillating behaviour accompanied with sharp shift peak (steep slope). This large spatial shift may provide an alternative strategy to develop novel sub-micrometric optical devices and biosensors.

Keywords: Goos–Hänchen shift, Imbert–Fedorov shift, α-MoO_3

PACS: 42.65.–k, 81.05.Xj, 77.22.Ch **DOI:** 10.1088/1674-1056/acd526

1. Introduction

A number of studies have shown that when a paraxial light beam interacts with the surface of the materials under specific conditions, the reflective beams show a relatively small shift from their geometrically/symmetrically incidence position.[1,2] The shift that occurs in the plane of the incoming light is referred to as the Goos–Hänchen (GH) shift, which was first observed by Goos and later confirmed experimentally by Hänchen.[3,4] While the shift normal to the plane of incident light is called the Imbert–Fedorov (IF) shift,[5,6] which further originates from the spin–orbit interaction of incident light.[7] The GH shift length is usually nearly the vacuum wavelength when the light–beam interacts with the conventional dielectrics, while the IF shift only indicates a small fraction of the vacuum wavelength.[2,8] It has been observed that the GH shift (in the case of the total internal reflection) is highly related to the medium-anisotropy.[3,5] Because of their excellent performance in micro-nano optics and device technology, these two phenomena have aroused wide interest of researchers. They used several materials to improve the spatial shifts of reflected light beam on the material surface, starting with the original work on isotropic and anisotropic mediums, such as the polar crystal,[9] photonic crystals,[8,10] metamaterials,[11] metasurfaces,[12] topological material,[13] magnetic media,[14] and quasibound states in the continuum.[15,16] When facing a small GH shift and IF shift, the quantum weak measurement can be used to detect this phenomenon veraciously, since it uses the precise measurement of the physical parameters of the material, such as dielectric function and permeability.[17] It accurately captures the shift produced on the surface of the material, opening up a broad window for the potential application of IF and GH shifts in sensing technology.

Hyperbolic materials (HMs) are materials with hyperbolic isofrequency contours, featuring having both positive sign and negative sign in their principal components of the dielectric permittivity tensor.[18–20] These materials have been utilized in various areas, including negative refraction,[21] hyperlens effect,[22] thermal emission engineering,[23] and other novelty optical devices.[24,25] Traditional HMs are based on meta-materials, which require careful design of the cells that make up a unit to obtain the characteristic hyperbolic permittivity tensor.[11] Despite the potential benefits of these strategies, their implementation poses significant challenges due to the complex and precise nano-fabrication and lithography

†Corresponding author. E-mail: shufangfu75@163.com
‡Corresponding author. E-mail: hsdzq80@126.com

© 2023 Chinese Physical Society and IOP Publishing Ltd

processes required to create a unit cell that can effectively manipulate light waves. Moreover, for the effective medium approximation to be valid, the unit cell must be considerably smaller than the wavelength of light. As a result, researchers have turned to explore natural biaxial hyperbolic material (NBHM), which possesses structural anisotropy resulting in hyperbolic permittivity without the need for lithography techniques.[26,27] For example, hexagonal boron nitride (hBN) has remarkable optical performance, featuring extremely low loss and two hyperbolic reststrahlen bands (HRBs) in the infrared range.[28,29] However, owing to its uniaxial optical response, it is unsuitable for in-plane anisotropy. On the other hand, α-molybdenum trioxide (α-MoO_3) exhibits phonon-driven NBHM behaviour in the long-wavelength mid-infrared range, making it a promising candidate for creating optical components with superior efficiency.[30,31]

α-MoO_3, a type of van der Waals crystal with orthorhombic unit cells, shows a biaxial hyperbolic anisotropy in the mid-infrared part of the electromagnetic spectrum.[32,33] The inherent anisotropy of α-MoO_3, arising from its distinctive crystalline structure, results in natural in-plane hyperbolic characteristics that stem from the interplay between the lattice modes and three crystal directions that are orthogonal to each other. Thus, this presents a novel possibility in the utilization of photonic tools that rely on the angle-dependent polarization, and opens the way for exploring polarization-based filters and reflectors.[34,35] Scholars have discovered that α-MoO_3 possesses various unique physical phenomena and applications. Hu *et al.*[36] documented the identification of both topological polaritons and photonic magic-angle in bi-layered α-MoO_3. Dereshgi and colleagues introduced a new approach to constructing IR polarization converters by using α-MoO_3 flakes, which does not involve lithography and purely relies on the use of orthogonal in-plane phonons.[37]

In this paper, we take the advantages of α-MoO_3 biaxial hyperbolicity and strong in-plane anisotropy to achieve an effective improvement of spatial shift. Meanwhile, we utilize the hBN as a substrate. As a natural hyperbolic material, the reststrahlen bands (RBs) of hBN partly overlap the RBs of α-MoO_3, and both the two hyperbolic materials exhibit hyperbolic dispersion characteristics in their frequency-response regions. Therefore, compared with ordinary isotropic and anisotropic materials, the hBN has a great ability to modulate the beam shifts.

2. Theoretical description

The setup comprises two distinct components: the surface layer, i.e., the α-MoO_3 film with thickness denoted by d, and the substrate that is a semi-infinite hBN crystal with its optical axis (OA) perpendicular to its surface. The schematic diagram of coordinate system and configuration can be found in Fig. 1, which shows that the orientation of the structure's surface is aligned with the x–y plane, while the plane of incidence is situated in the x–z plane. a, b, and c denote the [100], [010], and [001] principal-axis directions of α-MoO_3, respectively. The a axis lies in the surface plane at θ relative to the x axis, where θ can also be used to indicate the orientation of the incident plane. A Gaussian beam incident on the surface at angle β produces the shifts of reflected beam along the x axis and y axis, called GH and IF shifts, respectively.

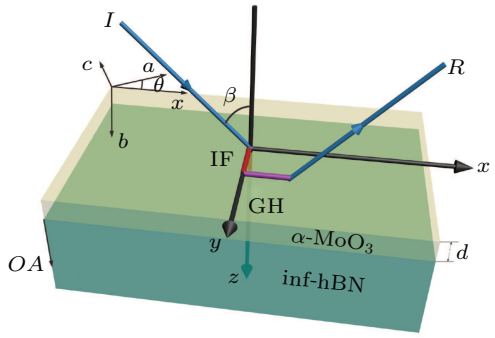


Fig. 1. Schematic illustrating geometry and coordination system, with β denoting the incident angle, θ the angle between incident plane and a–b plane, and d the thickness of α-MoO_3 layer.

In the o–abc coordination system, the dielectric permittivity of α-MoO_3 crystal is a diagonal matrix with elements ε_a, ε_b, and ε_c, which is an important characteristic of biaxial hyperbolic crystal. Nevertheless, the effective permittivity in the o–xyz coordinate system can be defined as

$$\varepsilon = \varepsilon_0 \begin{pmatrix} \varepsilon_{xx} & \varepsilon_{xy} & 0 \\ \varepsilon_{xy} & \varepsilon_{yy} & 0 \\ 0 & 0 & \varepsilon_c \end{pmatrix}, \tag{1}$$

where $\varepsilon_{xx} = \varepsilon_a \cos^2\theta + \varepsilon_b \sin^2\theta$, $\varepsilon_{yy} = \varepsilon_b \cos^2\theta + \varepsilon_a \sin^2\theta$, and $\varepsilon_{xy} = (\varepsilon_b - \varepsilon_a)\cos\theta \sin\theta$. The three dielectric constants can be collectively expressed as[19,38]

$$\varepsilon_j = \varepsilon_{\infty,j}\left(1 + \frac{\omega_{\mathrm{LO},j}^2 - \omega_{\mathrm{TO},j}^2}{\omega_{\mathrm{TO},j}^2 - \omega^2 - \mathrm{i}\omega\Gamma_j}\right), \quad j = a,b,c. \tag{2}$$

The permittivity tensor is denoted by ε_j, while $\varepsilon_{\infty,j}$ refers to the dielectric constant at high frequencies. In addition, there are damping constant Γ_j, longitudinal optical phonon frequency $\omega_{\mathrm{LO},j}$, and transverse $\omega_{\mathrm{TO},j}$ optical phonon frequency which are associated with the system. The parameters used in Eq. (2) are reproduced from Ref. [30].

For the α-MoO_3 layer, the induced electric field satisfies the following equation (based on Maxwell equations):

$$\boldsymbol{ME} = \begin{pmatrix} k_z^2 - \varepsilon_{xx} f^2 & -\varepsilon_{xy} f^2 & k_x k_z \\ -\varepsilon_{xy} f^2 & k_x^2 + k - \varepsilon_{yy} f^2 & 0 \\ k_x k_z & 0 & k_x^2 - \varepsilon_c f^2 \end{pmatrix} \begin{pmatrix} E_x \\ E_y \\ E_z \end{pmatrix} = 0, \tag{3}$$

where $f = \mu_0 \varepsilon_0 \omega^2$. Equation (3) has nontrivial solutions only when the $\det(\boldsymbol{M}) = 0$, it provides the well-known Fresnel's equation for biaxial medium, a quadratic equation, in the

squared z component of the wave vector, k_z, which is the two wave branches in the α-MoO_3. Its solutions k_z read as

$$k_{\pm}^2 = \frac{1}{2\varepsilon_c}(-b \pm \sqrt{b^2 - 4\varepsilon_c c}), \tag{4}$$

with $b = \varepsilon_{xx}(k_x^2 - \varepsilon_c f^2) + \varepsilon_c(k_x^2 - \varepsilon_{yy} f^2)$, and $c = \left(k_x^2 - \varepsilon_c f^2\right)\left(\varepsilon_{xx} k_x^2 - \varepsilon_{xx}\varepsilon_{yy} f^2 + \varepsilon_{xy}^2 f^2\right)$. In the substrate material, there are two wave vectors respectively usual wave $k_{\rm o}$ and unusual wave $k_{\rm e}$. Owing to the strong anisotropy of the α-MoO_3, the three electric field components combine. Hence, we can use Eq. (1) to rewrite the x and z components as functions of the y component, i.e., $E_x^{\pm} = (k_x^2 + k_{\pm}^2 - \varepsilon_{yy} f^2)/\varepsilon_{xy} f^2 = \Lambda_{\pm} E_y^{\pm}$ and $E_z^{\pm} = k_{\pm} k_x \Lambda_{\pm}/(\varepsilon_c f^2 - k_x^2) E_y^{\pm}$, for the two wave branches in the α-MoO_3. Therefore, the electric field can be expended only in the y component in the α-MoO_3 and will be written as follows:

$$E_{x,y} = E_{x,y}^{\rm I} \mathrm{e}^{\mathrm{i}k_z z} + E_{x,y}^{\rm R} \mathrm{e}^{-\mathrm{i}k_z z}, \quad (z < 0), \tag{5a}$$

$$E_y = A\mathrm{e}^{\mathrm{i}k_+ z} + B\mathrm{e}^{-\mathrm{i}k_+ z} + C\mathrm{e}^{\mathrm{i}k_- z} + D\mathrm{e}^{-\mathrm{i}k_- z}, \quad (0 < z < d), \tag{5b}$$

$$E_x = F_x \mathrm{e}^{\mathrm{i}k_{\rm e} z}, \quad E_y = F_y \mathrm{e}^{\mathrm{i}k_{\rm o} z}, \quad (z > d), \tag{5c}$$

where superscript I represents the incident light and R represents the reflection light, where the common factor $\exp(\mathrm{i}k_x x - \mathrm{i}\omega t)$ is omitted for simplicity, $k_{\rm o}$ and $k_{\rm e}$ denote the usual light wave vector and unusual light wave vector in the hBN, respectively. Meanwhile, the magnetic fields can be achieved with the Maxwell equation in the different spaces. Subsequently, the boundary conditions are introduced, which stipulate that the in-plane segments of the magnetic field and electric field must be seamless across the film's surface, located at $z = 0$ and d. The electric field's amplitude is determined by

$$\begin{pmatrix} E_y^{\rm I} \\ E_y^{\rm R} \\ E_x^{\rm I} \\ E_x^{\rm R} \end{pmatrix} = \frac{1}{2}\begin{pmatrix} 1+k_+/k_z & 1-k_+/k_z & 1+k_-/k_z & 1-k_-/k_z \\ 1-k_+/k_z & 1+k_+/k_z & 1-k_-/k_z & 1+k_-/k_z \\ \Lambda_+ + \lambda_+ & \Lambda_+ - \lambda_+ & \Lambda_- + \lambda_- & \Lambda_- - \lambda_- \\ \Lambda_+ - \lambda_+ & \Lambda_+ + \lambda_+ & \Lambda_- - \lambda_- & \Lambda_- + \lambda_- \end{pmatrix} \begin{pmatrix} A \\ B \\ C \\ D \end{pmatrix} = T_1 \begin{pmatrix} A \\ B \\ C \\ D \end{pmatrix}, \tag{6a}$$

$$\begin{pmatrix} F_y \\ 0 \\ F_x \\ 0 \end{pmatrix} = \frac{1}{2}\begin{pmatrix} 1+k_+/k_{\rm o} & 1-k_+/k_{\rm o} & 1+k_-/k_{\rm o} & 1-k_-/k_{\rm o} \\ 1-k_+/k_{\rm o} & 1+k_+/k_{\rm o} & 1-k_-/k_{\rm o} & 1+k_-/k_{\rm o} \\ \Lambda_+ + \gamma_+ & \Lambda_+ - \gamma_+ & \Lambda_- + \gamma_- & \Lambda_- - \gamma_- \\ \Lambda_+ - \gamma_+ & \Lambda_+ + \gamma_+ & \Lambda_- - \gamma_- & \Lambda_- + \gamma_- \end{pmatrix} P \begin{pmatrix} A \\ B \\ C \\ D \end{pmatrix} = T_2 P \begin{pmatrix} A \\ B \\ C \\ D \end{pmatrix}, \tag{6b}$$

with

$$\lambda_{\pm} = k_{\pm} k_z \varepsilon_c \Lambda_{\pm}/(\varepsilon_{\rm c} f^2 - k_z^2),$$
$$\gamma_{\pm} = k_{\pm} k_{\rm e} \varepsilon_c \Lambda_{\pm}/[\varepsilon_t(\varepsilon_c f^2 + k_z^2)].$$

The P is a diagonal matrix[$\mathrm{e}^{\mathrm{i}k_+ z}$, $\mathrm{e}^{-\mathrm{i}k_+ z}$, $\mathrm{e}^{\mathrm{i}k_- z}$, $\mathrm{e}^{-\mathrm{i}k_- z}$]. After eliminating the A, B, C, and D amplitudes, we can obtain $E_{x,y}^{\rm I,R} = TF_{x,y} = T_1 T_2^{-1} F_{x,y}$. By using T_{mn} to indicate different elements of the matrix T, the reflected electric field can be written as

$$\begin{aligned} E_y^{\rm R} &= \frac{T_{11}T_{23} - T_{21}T_{13}}{T_{11}T_{33} - T_{13}T_{31}} E_x^{\rm I} + \frac{T_{21}T_{33} - T_{23}T_{31}}{T_{11}T_{33} - T_{13}T_{31}} E_y^{\rm I} \\ &= a_{11} E_x^{\rm I} + a_{22} E_y^{\rm I}, \end{aligned} \tag{7a}$$

$$\begin{aligned} E_x^{\rm R} &= \frac{T_{11}T_{43} - T_{41}T_{13}}{T_{11}T_{33} - T_{13}T_{31}} E_x^{\rm I} + \frac{T_{41}T_{33} - T_{43}T_{31}}{T_{11}T_{33} - T_{13}T_{31}} E_y^{\rm I} \\ &= a_{21} E_x^{\rm I} + a_{22} E_y^{\rm I}, \end{aligned} \tag{7b}$$

while the reflective electric field (z-component) can be denoted by $E_z^{\rm R} = \tan(\beta) E_x^{\rm R}$.

The amplitude of the electric field for the transverse electric (TE) wave with s-polarization is represented by $E_y^{\rm R}$, while in the reflected beam, the two components of the field amplitude for the transverse magnetic (TM) wave with p-polarization are denoted by $E_x^{\rm R}$ and $E_z^{\rm R}$. The reflective electric field is expressed as a matrix form in the o–xyz coordinate system. To resolve the GH shift and IF shift in the reflective beam, it is essential to employ rotational transformations on both the incident and reflective central waves. According to the geometric correlation, the transformation relationship between the incident electric field and reflected electric field can be obtained as follows: $E_x^{\rm I} = E_{\rm p}^{\rm I}\cos(\beta)$, $E_y^{\rm I} = E_{\rm s}^{\rm I}$, $E_z^{\rm I} = -E_{\rm p}^{\rm I}\sin(\beta)$, $E_{\rm p}^{\rm R} = -E_x^{\rm R}\cos(\beta) - E_z^{\rm R}\sin(\beta)$, $E_{\rm s}^{\rm R} = E_y^{\rm R}$, and $E_z^{\rm R} = \cot(\beta) E_x^{\rm R}$. As result, the correlation equation for the incident field and reflective field in the beam coordinate system can be written as

$$\begin{pmatrix} E_{\rm p}^{\rm R} \\ E_{\rm s}^{\rm R} \end{pmatrix} = \begin{pmatrix} -a_{11} & -\dfrac{a_{12}}{\cos(\beta)} \\ a_{21}\cos(\beta) & a_{22} \end{pmatrix} \begin{pmatrix} E_{\rm p}^{\rm I} \\ E_{\rm s}^{\rm I} \end{pmatrix}. \tag{8}$$

The subscripts "s" and "p" indicate the s-polarization and p-polarization of the incident and reflected central waves, respectively. While the results mentioned earlier are obtained by using the central plane wave; if we consider the paraxial wave, the incident beam is limited to a narrow range of plane waves around the central wave in momentum space. We assume the incident beam to be a Gaussian beam, which does not comply with the law of reflection Eq. (8) and provides two indications: firstly, the use of α-MoO_3 results in a non-diagonal matrix relationship between the incident electric field and re-

flected electric field, and secondly, all elements of the reflection coefficient matrix are dependent on θ and β. If this arises from the anisotropy of the α-MoO_3 layer, it can be anticipated that the GH and IF shift may exist for a linearly-polarized incident beam. In this case, the expression for the GH shift should be derived. To do so, we can expand the elements of the coefficient-matrix to the first order of β_p in Eq. (8) and solely consider β_p while ignoring θ_s. The relative reflection may be expressed as

$$\begin{pmatrix} E_p^R \\ E_s^R \end{pmatrix} = \begin{pmatrix} -(a_{11}+a'_{11}\beta_p) & -\dfrac{a_{12}+a'_{12}\beta_p}{\cos(\beta)} \\ (a_{21}+a'_{21}\beta_p)\cos(\beta) & a_{22}+a'_{22}\beta_p \end{pmatrix} \begin{pmatrix} E_p^I \\ E_s^I \end{pmatrix}. \quad (9)$$

The term "prime" refers to the derivative of β. Hence, the explanation of the GH shift is provided by

$$\Delta_{GH} = \frac{1}{2\pi k_0 Q} \mathrm{Im}\left\langle \boldsymbol{E}^R \middle| \frac{\partial}{\partial \beta_p} \boldsymbol{E}^R \right\rangle, \quad (10)$$

with $\boldsymbol{E}^R = E_p^R + E_s^R$ and $Q = \left|\boldsymbol{E}^R\right|^2$.

First, We focus our attention on deriving the IF shift formula. The polarization orientation of the incident or reflected beam is directly changed by a slight adjustment in the incident plane's orientation. The matrix components in Eq. (8), where only θ_s is considered and β_p is omitted, are also affected. For smaller rotation θ_s, the reflected electric field can be written as

$$\begin{pmatrix} E_p^R \\ E_s^R \end{pmatrix} = \begin{pmatrix} s_{11} & s_{12} \\ s_{21} & s_{22} \end{pmatrix} \begin{pmatrix} E_p^I \\ E_s^I \end{pmatrix}. \quad (11)$$

The IF shift is calculated numerically based on Eq. (11) and its derivative, and defined as

$$\Delta_{IF} = -\frac{1}{2\pi k_0 Q \sin(\beta)} \mathrm{Im}\left\langle \boldsymbol{E}^R \middle| \frac{\partial}{\partial \theta_s} \boldsymbol{E}^R \right\rangle. \quad (12)$$

If the surface layer and substrate are replayed by an isotropic material, the matrix elements of Eq. (8) will become $a_{12} = a_{21} = 0$, $a_{11} = -f_p$, and $a_{22} = f_s$ (where f_p and f_s are the reflective coefficients of the p and s waves). For the high-symmetry configurations ($\theta = 0, 90^\circ$), the same results can be obtained: $a_{12} = a_{21} = 0$, $a_{11} = -f_p$, and $a_{22} = f_s$. Likewise, the expression of GH and IF shifts in the isotropic medium can be obtained with the same method. Consequently, equations (10) and (12) can be simplified into a well-known result, which is cited from Ref. [1].

3. Numerical calculations and discussion

To find out the spatial shift of the surface of the α-MoO_3 crystal, we first illustrate the permittivity of the monolayer α-MoO_3 crystal as depicted in Fig. 2(a), where ε_a, ε_b, and ε_c represent the three elements of dielectric permittivity of α-MoO_3 crystal in the a, b, and c directions, respectively. If there exists an frequency interval where the signs of dielectric functions are opposite, this frequency interval is called an HRB. For the NBHM, if one element has a positive dielectric function value and the other two elements have negative dielectric function values, it is called a type-II hyperbolic material, otherwise it is a type-I hyperbolic. Therefore, we can see the five HRBs of α-MoO_3 with different colors, as listed in Table 1.

Table 1. Frequency regions, properties and relations among ε_a, ε_b, and ε_c of types α-MoO_3.

Color regions	Frequency range (cm^{-1})	Properties and relations of α-MoO_3	Types
Magenta	$545 < \omega < 820$	$\varepsilon_a < 0, \varepsilon_b > \varepsilon_c > 0$	I
Blue	$820 < \omega < 851$	$\varepsilon_b < \varepsilon_a < 0, \varepsilon_c > 0$	II
Cyan	$851 < \omega < 951$	$\varepsilon_b < 0, \varepsilon_c > \varepsilon_a > 0$	I
Green	$951 < \omega < 972$	$\varepsilon_c < \varepsilon_b < 0, \varepsilon_a > 0$	II
Yellow	$972 < \omega < 1004$	$\varepsilon_c < 0, \varepsilon_a > \varepsilon_b > 0$	I

The physical parameters of the hBN crystal are presented in Ref. [11]. Its permittivity values are illustrated in Fig. 2(b), where the red part corresponds to the HRB-I, and the green part refers to the HRB-II. Furthermore, we can observe that the HRB-I of hBN and the second HRB of α-MoO_3 partly overlap in a frequency response space. Both materials exhibit unique properties in this common region, so we will focus our attention on this area.

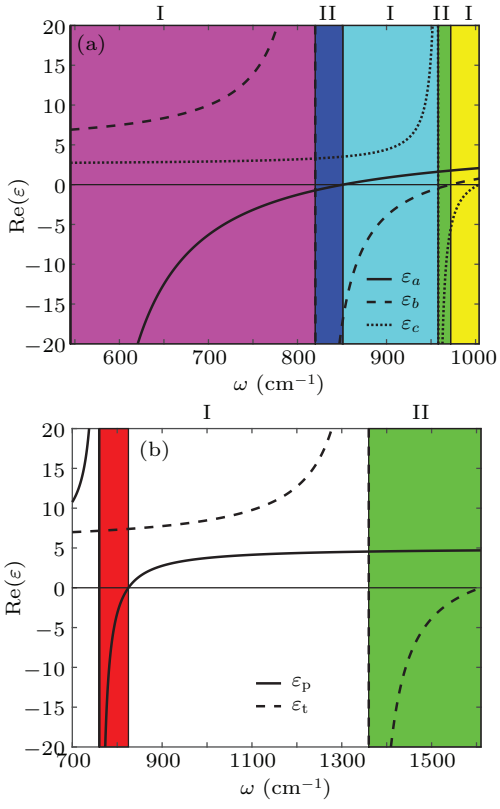


Fig. 2. (a) Permittivity of monolayer α-MoO_3, with solid, dashed, and dotted lines denoting the permittivity in different crystal directions, and different areas relating to different HRBs. (b) Permittivity of the bulk hBN, with solid and dashed lines referring to the permittivity parallel and vertical to OA, and red and green areas indicating HRBs respectively.

To comprehend the shift spectrum in the reflected beam spectra, it is necessary to revisit the reflection and transmission that occur at the interface between air and an isotropic polar crystal with a relative permittivity ε. When k_z becomes imaginary, the total reflection is observed, and the transmitted wave transforms into an evanescent wave. Then, the critical angle is determined by the equation $\sin^2\beta_c = \varepsilon$, where $0 < \varepsilon < 1$. The Brewster angle can be determined by $R_{\rm p} = 0$. For the present structure, a similar definition for the critical or Brewster angle can still be achieved.

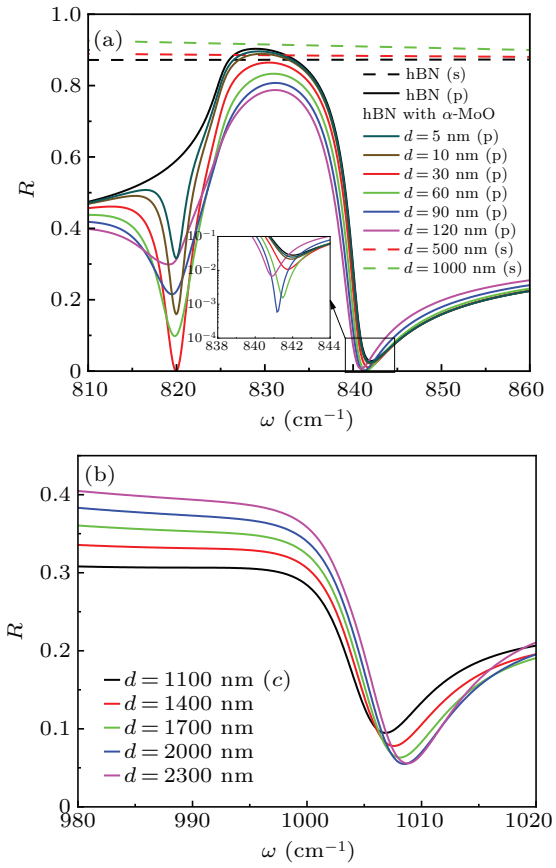


Fig. 3. Curves of reflectivity corresponding to (a) linearly-polarized incident beam and (b) circularly-polarized incident beam at different frequencies and thickness values of α-MoO_3. In panel (a), the green dashed line is related to the s-polarization incident beam, and the solid line corresponds to the p-incident beam. The inset illustrates the reflective ratio when $d < 30$ nm for p-polarized incident beam.

Figure 3 shows the curves of reflectance of the p-polarized, s-polarized, and circularly polarized beams. The black solid line or dash line in Fig. 3(a) indicates the reflectivity of the surface of semi-infinite hBN material without the α-MoO_3 film for p- or s-polarized incident beam. It is not difficult to find that the reflectivity of p-polarized incident beam changes significantly with frequency, while the reflectivity of s-polarized incident beam remains basically unchanged. After placing the α-MoO_3 film on hBN, two dips are observed at $\omega \approx 820$ cm^{-1} and 840 cm^{-1}, respectively. In addition, the reflectivity of p-polarized incident beam approaches to zero at $\omega \approx 840$ cm^{-1}, where the incident angle should be the Brewster's angle. Normally, the spatial shifts, such as GH shift and IF shift, can be enhanced greatly at critical angle or Brewster's angle.[12] An inset about the reflectivity at $\omega \approx 840$ cm^{-1} is plotted in order to further examine the effect of the thickness of α-MoO_3 film on the reflectivity. It is clear to find that the reflectivity will be larger than 1% once the the thickness of α-MoO_3 film is less than 30 nm. It can be predicted that if the larger GH or IF shift is expected, the thickness of α-MoO_3 film should be larger than 30 nm. On the other hand, the reflectivity for s-polarized incident beam remains unchanged with the frequency even if the α-MoO_3 film is placed on the surface of hBN, while the reflectivity increases slightly with the thickness of α-MoO_3 film increasing. Comparing with Fig. 2(b), it also can be found that the permittivity of hBN $\varepsilon_{\rm p}$ is just equal to 1.0 at $\omega \approx 40$ cm^{-1} for p-polarized incident beam, which is located near the epsilon being nearly zero of HRB-I. Therefore, we will focus our attention on the GH or IF shift of p-polarized incident beam in the following discussions. Figure 3(b) displays the curves of reflectivity of left c-polarized incident beam for α-MoO_3 films with different thickness values. Only one dip appears at $\omega \approx 1007$ cm^{-1} where the reflectivity gradually decreases with the increase of α-MoO_3 film increasing.

Initially, we concentrate on two highly symmetric configurations, namely, geometry-I ($\theta = 0°$) with the a axis of α-MoO_3 along the x axis, and geometry-II ($\theta = 90°$) with the a axis perpendicular to the x axis. For the highly symmetric configurations, $\varepsilon_{xy} = 0$ in Eq. (4) which leads to an analytical expression for $k_\pm$. $k_\pm^2 = \varepsilon_{yy} f^2 - k_x^2$ for s-polarized incident beam and $\varepsilon_{zz} k_\pm^2 = \varepsilon_{xx}\varepsilon_{zz} f^2 - \varepsilon_{xx} k_x^2$ for p-polarized incident beam. In geometry-I, $\varepsilon_{xx} = \varepsilon_a$, $\varepsilon_{yy} = \varepsilon_b$, and in geometry-II, $\varepsilon_{xx} = \varepsilon_b$, $\varepsilon_{yy} = \varepsilon_a$. Figure 4 illustrates the curves of GH shift versus frequency for the different thickness in the geometry-I and geometry-II. The GH shift on the surface of hBN is presented in Fig. 4(a), which is about $5\lambda_0$ at $\omega = 841.5$ cm^{-1}. With the increase of the thickness of α-MoO_3 film, the influence of thickness on GH shift becomes more pronounced. The GH shift reaches a negative maximum value of about $39\lambda_0$ at $d = 90$ nm. Of course, if the positive GH shift is required we have to consider the situation at $d = 120$ nm. The corresponding frequency is located on the left border of the overlapping region of HRBs. In Fig. 4(b), a noticeable peak for GH shift is present in geometry-II, where a maximum GH shift can reach $86\lambda_0$ and rapidly changes from negative to positive. It further proves that the GH shift can be enhanced significantly at the Brewster angle since a phase gradient of the corresponding reflection coefficient will experience a sharp variation due to the high in-plane anisotropy. For both geometries, it can be found that the GH shift generated on the the surface of α-MoO_3-hBN is much larger than the one excited on the surface of the semi-infinite hBN. As is well known, according to the discussion of Eq. (12) the IF shift cannot be generated for linearly polarized

incident beam at the interface between two isotropic media. However, the α-MoO_3 layer leads to the off-diagonal relationship between the incident electric field and reflective field as demonstrated in Eq. (9). We can predict that the IF shift will be generated not only by the circularly polarized beam but also by the linearly polarized beam, which is caused mainly by the in-plane anisotropy of α-MoO_3 layer. In order to investigate the IF shift for p-polarized incident beam, we illustrate the variation of IF shift in the θ–ω plane at $\beta = 12°$ as shown in Fig. 4(c). It is obvious that the larger IF shift exits in the region of $13° < \theta < 50°$ where the incident frequency is fixed at about 825 cm^{-1}. Moreover, the largest IF shift can be about $0.07\lambda_0$ at $\theta = 33°$. When $\theta = 0°$ and 90°, the off-diagonal elements of the reflection coefficient matrix become zero, which will cause the reflected beam to become a single s- or p-polarized beam. Thus, the IF shift still cannot be observed at the two highly symmetric structures, which can also be illustrated by Fig. 4(c).

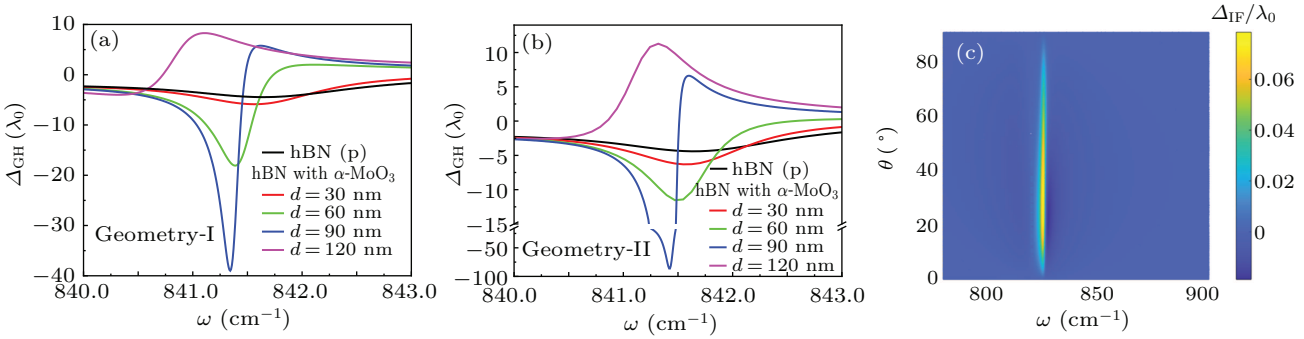


Fig. 4. Curves of GH shift and IF shift of reflective beam for α-MoO_3 with various thicknesses in the HRBs in (a) geometry-I, and ((b), (d)) geometry-II for p-polarized incident beam with $\beta = 85°$, with solid black line referring to GH shift on the semi-infinite hBN. (c) IF shift versus and frequency for p-polarized incident angle with $\beta = 12°$.

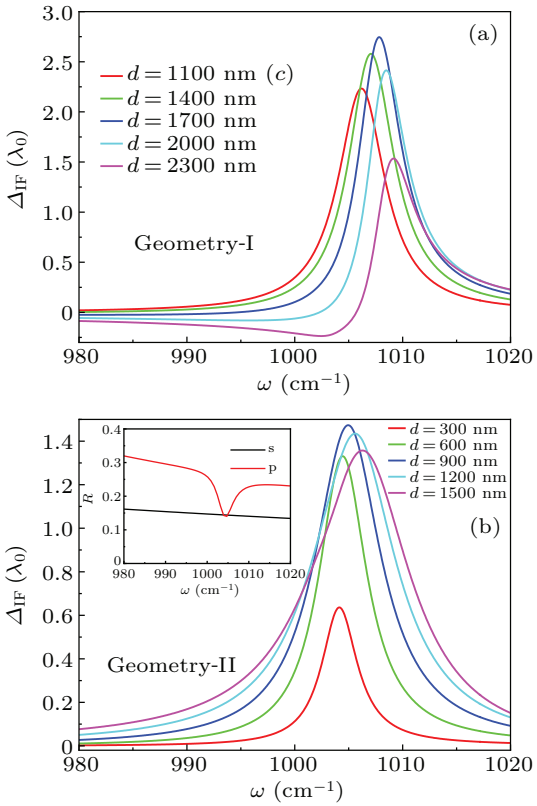


Fig. 5. Curves of IF shift of reflective beam of α-MoO_3 with various thicknesses in HRBs in (a) geometry-I and (b) geometry-II for the circularly polarized incident beams with $\beta = 12°$.

In the previous discussion, we described in detail the GH and IF shifts of p-polarized incident beam. Generally speaking, the generation of IF shift is attributed to the conservation of spin–orbit angular momentum. Therefore, we choose the left circularly-polarized incident beam to simulate the IF shift. In Fig. 5, the peak of the IF shift can be seen at $\omega = 1007$ cm^{-1}, corresponding to $\varepsilon_c = 0$. In addition, as the thickness of α-MoO_3 increases, the maximum value of the IF shift first increases and then decreases. When $d = 1700$ nm, the maximum IF shift can reach about $2.7\lambda_0$. This pattern can also be seen in geometry-II as shown in Fig. 5(b). When the thickness is 900 nm, the peak of the IF shift is about $1.4\lambda_0$. In order to analyze the peak of the IF shift, which is taken for example, we simulate the reflectivity of the s- and p-polarized incident beams in geometry-II when $d = 900$ nm, which is shown in the inset of Fig. 5(b). A dip of R_p is observed which just intersects with R_s at $\omega = 1007$ cm^{-1}. Based on the discussions in Ref. [11], the conditions reaching the maximum value of IF shift should be satisfied at this frequency.

4. Conclusions

To sum up, our investigation focuses on analyzing the shift of the reflected beam from the α-MoO_3 with a finite thickness on a bulk hBN substrate. We observed that the interplay between anisotropic hyperbolic polaritons in α-MoO_3 plates and hBN crystal results in intricate changes in the GH and IF spectra. They are not like the reflected beam from the bulk hBN crystal surface nor the infinite thickness α-MoO_3 surface. Especially for geometry-II, the GH shift can reach $86\lambda_0$ with $d = 90$ nm, which lies in the Brewster angle. By comparing the GH shift of the added MoO_3 flakes with that of the semi-infinite hBN structure, adding MoO_3 flakes with a certain thickness can effectively increase the GH shift of the surface in this frequency interval. For the circularly-polarized

incident beam, the IF shift is $2.7\lambda_0$ when the NBHM thickness is 1700 nm. Meanwhile, both materials are NBHM, which are easier to prepare and have simpler structures. These findings pave the way for future research into modulating the GH and IF shifts, which can be used to create novel micro-optical devices and biosensors.

Acknowledgements

Project supported by the Natural Science Foundation of Heilongjiang Province, China (Grant No. LH2020A014), the Fund from the Education Commission of Heilongjiang Province, China (Grant No. 2020-KYYWF352), the Fund from the Key Laboratory of Engineering Dielectrics and Its Application (Harbin University of Science and Technology), Ministry of Education, China (Grant Nos. KFM202005 and KF20171110), and the Harbin Normal University Postgraduate Innovative Research Project, Heilongjiang Province, China (Grant Nos. HSDSSCX2022-53 and HSDSSCX2022-49).

References

[1] Bliokh K Y and Aiello A 2013 *J. Opt.* **15** 014001
[2] Li C F 2007 *Phys. Rev. A* **76** 013811
[3] Goos F and Hänchen H 1947 *Ann. Phys.* **436** 333
[4] Goos F and Hänchen H 1949 *Ann. Phys.* **5** 251
[5] Imbert C 1972 *Phys. Rev. D* **5** 787
[6] Fedorov F I 2013 *J. Opt.* **15** 014002
[7] Takayama O, Sukham J, Malureanu R, Lavrinenko A V and Puentes G 2018 *P Opt. Lett.* **43** 004602
[8] Soboleva I V, Moskalenko V V and Fedyanin A A 2012 *Phys. Rev. Lett.* **108** 123901
[9] Zhang Q, Zhou S, Fu S F and Wang X Z 2019 *J. Opt. Soc. Am. B* **36** 1429
[10] Petrov N I, Danilov V A, Popov V V and Usievich B A 2020 *Opt. Express* **28** 7552
[11] Song H Y, Fu S F, Zhang Q, Zhou S and Wang X Z 2021 *Opt. Express* **29** 19068
[12] Peng H Y and Wang X Z 2021 *J. Opt. Soc. Am. B* **38** 2027
[13] Liu S Q, Song Y F, Wan T, Ke Y G and Luo Z M 2022 *Chin. Phys. B* **31** 074101
[14] Fu S F, Wang X G, Zhang Y Q, Zhou S and Wang X Z 2021 *Opt. Express* **29** 39125
[15] Wu F, Luo M, Wu J, Fan C, Qi X, Jian Y, Liu D, Xiao S Y, Chen G Y, Jiang H T, Sun Y and Chen H 2021 *Phys. Rev. A* **104** 023518
[16] Wu F, Wu J J, Guo Z W, Jiang H T, Sun Y, Li Y H, Ren J and Chen H 2019 *Phys. Rev. Appl.* **12** 014028
[17] Hosten O and Kwiat P 2008 *Science* **319** 787
[18] Poddubny A, Iorsh I, Belov P and Kivshar Y 2013 *Nat. Photon.* **7** 948
[19] Drachev V P, Podolskiy V A and Kildishev A V 2013 *Opt. Express* **21** 15048
[20] Shekhar P, Atkinson J and Jacob Z 2014 *Nano Converg.* **1** 14
[21] Yao J, Liu Z, Liu Y, Wang Y, Sun C, Bartal G, Stacy A M and Zhang X 2008 *Science* **321** 930
[22] Lee H, Liu Z, Xiong Y, Sun C and Zhang X 2007 *Opt. Express* **15** 15886
[23] Guo Y, Cortes C L, Molesky S and Jacob Z 2012 *Appl. Phys. Lett.* **101** 131106
[24] Pujol-Closa P, Gomis-Bresco J, Mukherjee S, Gómez-Díaz J S, Torner L and Artigas D 2021 *Opt. Lett.* **46** 58
[25] Xu G, Pan T, Zang T and Sun J 2008 *Opt. Commun.* **281** 2819
[26] Korzeb K, Gajc M and Pawlak D A 2015 *Opt. Express* **23** 25406
[27] Gjerding M N, Petersen R, Pedersen T G, Mortensen N A and Thygesen K S 2017 *Nat. Commun.* **8** 320
[28] Wu X H 2018 *Plasmonics* **13** 1695
[29] Li Y B, Song H Y, Zhang Y Q, Wang X G, Fu S F and Wang X Z 2022 *Chin. Phys. B* **31** 064207
[30] Deng G, Dereshgi S A, Song X, Wei C and Aydin K 2020 *Phys. Rev. B* **102** 035408
[31] Sui C, Liu Y, Wang X G, Zhou S, Fu S F, Wang X, Zhang Q, Liang H and Wang X Z 2022 *J. Opt. Soc. Am. B* **39** 900
[32] Ma W, Alonso-González P, Li S, Nikitin A Y, Yuan J, Martín-Sánchez J, Taboada-Gutiérrez J, Amenabar I, Li P, Vélez S, Tollan C, Dai Z, Zhang Y, Sriram S, Kalantar-Zadeh K, Lee S T, Hillenbrand R and Bao Q 2018 *Nature* **562** 557
[33] Kim J H, Dash J K, Kwon J, Hyun C, Kim H, Ji E and Lee G H 2019 *2D. Mater.* **6** 015016
[34] Wei C, Abedini Dereshgi S, Song X, Murthy A, Dravid V P, Cao T and Aydin K 2020 *Adv. Opt. Mater.* **8** 2000088
[35] Wu B Y, Shi Z X, Wu F, Wang M J and Wu X H 2022 *Chin. Phys. B* **31** 044101
[36] Hu G, Ou Q, Si G, Wu Y, Wu J, Dai Z, Krasnok A, Mazor Y, Zhang Q, Bao Q, Qiu C W and Alù A 2020 *Nature* **582** 209
[37] Abedini Dereshgi S, Folland T G, Murthy A A, Song X, Tanriover I, Dravid V P, Caldwell J D and Aydin K 2020 *Nat. Commun.* **11** 5771
[38] Kildishev A V, Boltasseva A and Shalaev V M 2013 *Science* **339** 1232009
[39] Song H Y, Chen Z X, Li Y B, Hao S P, Zhang Q, Zhou S, Fu S F and Wang X Z 2023 *J. Opt. Soc. Am. B* **40** 488686